Journal of
Synchrotron
Radiation

ISSN 0909-0495

Received 25 November 2010
Accepted 26 April 2011

Calculation of anisotropic properties of dental enamel from synchrotron data

Lars Raue* and Helmut Klein

GZG, Department of Crystallography, Georg-August-University of Göttingen, Göttingen, Germany.
E-mail: lraue@uni-goettingen.de

Obtaining information about the intrinsic structure of polycrystalline materials is of prime importance owing to the anisotropic behaviour of individual crystallites. Grain orientation and its statistical distribution, *i.e.* the texture, have an important influence on the material properties. Crystallographic orientations play an important role in all kinds of polycrystalline materials such as metallic, geological and biological. Using synchrotron diffraction techniques the texture can be measured with high local and angular resolving power. Here methods are presented which allow the spatial orientation of the crystallites to be determined and information about the anisotropy of mechanical properties, such as elastic modulus or thermal expansion, to obtained. The methods are adapted to all crystal and several sample symmetries as well as to different phases, for example with overlapping diffraction peaks. To demonstrate the abilities of the methods, human dental enamel has been chosen, showing even overlapping diffraction peaks. Likewise it is of special interest to learn more about the orientation and anisotropic properties of dental enamel, since only basic information is available up to now. The texture of enamel has been found to be a tilted fibre texture of high strength (up to 12.5×). The calculated elastic modulus is up to 155 GPa and the thermal expansion up to $22.3 \times 10^{-6}\,^{\circ}\mathrm{C}^{-1}$.

Keywords: texture; anisotropy; elastic modulus; thermal expansion; enamel; tooth; hydroxylapatite.

1. Introduction

The majority of all technological, geological and biological materials have a polycrystalline structure. They are composed of crystallites which are anisotropic with respect to many of their physical and mechanical properties. The macroscopic properties of such materials may be anisotropic if the orientation distribution of the crystallites is not completely random. Hence the macroscopic anisotropy and the materials' properties are mainly determined by the single-crystal anisotropy and the orientation distribution function of these crystallites (Bunge, 1993). Nevertheless, the direction dependence of macroscopic properties can also depend on, for example, crystallite shape, pore structures or cracks. In technologically used materials the macroscopic properties play a special role. The property profile of such materials has to be adapted to the application profile in a work piece. Similarly, the same is valid for biological materials. Since most biomaterials have been improved over millions of years, it does not astonish that the macroscopic properties of such materials are normally highly adapted to the mechanical needs such a material has to fulfil. In order to understand the physical behaviour of a polycrystalline biomaterial, examination methods of technological materials can be used. In recent years diffraction techniques using high-energy synchrotron radiation has become more and more important for material sciences because of their excellent properties such as high angular and local resolving power, high brilliance and high penetration depth (Heidelbach *et al.*, 1999; Wcislak *et al.*, 2001, 2002; Lonardelli *et al.*, 2005; Klein, 2009). The investigations described here were carried out using the multi-purpose diffraction device at beamline BW5 at HASYLAB/DESY in Hamburg, Germany.

The material used in this investigation was dental enamel from a human incisor tooth. The anisotropic properties of this biomaterial are of prime importance since the mechanical properties of materials used to fill cavities differ significantly from those of the dental enamel itself (Chudoba *et al.*, 2005). In the worst case the filling of a tooth can damage the enamel of a tooth of the opposite side; hence, when applying mechanical loads (*e.g.* during chewing) the property profiles of both materials, *i.e.* the enamel and the filling material, can be very different, such that a harder filling can abrase the softer enamel of a healthy tooth. There are not only problems with the hardness, however. Fillings can also shrink or expand since the coefficients of thermal expansion differ from those of the enamel itself. All this could be avoided if the anisotropic properties of dental enamel could be known in detail, hence then a filling material with suitable properties could be sought

or fabricated as an equivalent replacement for the dental enamel. To find such a proper material, the anisotropic macroscopic properties of dental enamel must be determined first in detail.

2. Sample material

Teeth consist generally of two main structural components (Fig. 1): the upper part (crown) is covered by dental enamel, followed by dentine and the pulp with blood vessels and nerves; the lower part (root) with its cementum stabilizes the tooth in the bone of the jaw.

Dental enamel is the most highly mineralized and hardest biological tissue in the human body (Dorozhkin, 2007). It is made of hydroxylapatite (HAP), $Ca_5(PO_4)_3(OH)$, which is hexagonal (6/*m*). The lattice parameters are a = 9.418 Å and c = 6.875 Å.

Human dental enamel has been chosen as the object of our investigation because it is important to determine the orientation of the crystallites within, since this orientation controls the anisotropy of mechanical properties such as the elastic modulus or the thermal expansion (Bunge, 1993; Nye, 1985; Park *et al.*, 2001).

The examined human tooth was the right first upper incisor, tooth 11 according to the nomenclature of the world dental federation (FDI; Fédération Dentaire Internationale). This tooth was originally used for another study about the periodontal ligament, approved by the local ethics committee. A 0.5 mm-thick slice of the front part was cut using a diamond saw so that the sample only consists of enamel without the inner dentine. To measure the local change of the HAP orientations a measurement grid was constructed with 15 points in a horizontal line and 12 points in a vertical line (see Fig. 2). The filled square indicates the position of the example data point for which the Rietveld refinement and texture analysis is also shown in detail. For all other grid points only the results of the texture analysis and calculations of the elastic modulus and the thermal expansion are presented.

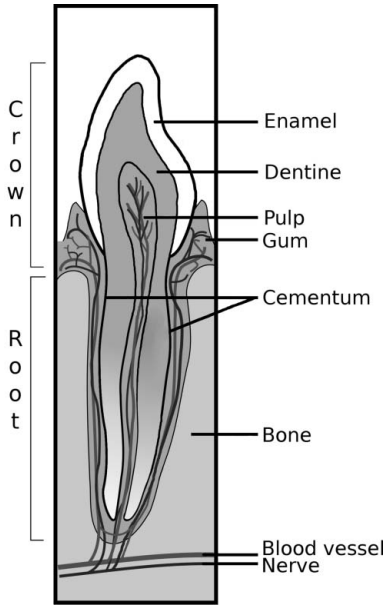

Figure 1
Schematic cross section of a human incisor tooth.

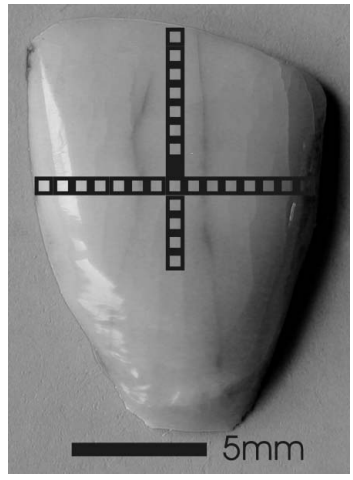

Figure 2
Upper incisor tooth with the position of the overlaying measuring grid. The filled square indicates the position of the grid point for which the process of analysis is shown in detail.

3. Experimental method

The texture measurements were carried out at the high-energy synchrotron beamline BW5 at HASYLAB/DESY in Hamburg, Germany. The instrument was equipped with a mar345 on-line image-plate area detector for the diffraction-image registration, an ω-stage for sample orientation, and two linear stages (X- and Z-direction) for local texture analysis (Fig. 3). Particular features of texture measurements with this instrument are the high angular resolution in Bragg angle and in the crystal orientation, the high beam intensity and the high penetration depth. A SiGe (111) gradient crystal monochromator and an energy of ~100 keV (λ = 0.1255 Å) were used. The cross section of the monochromatic beam was 0.5 ×

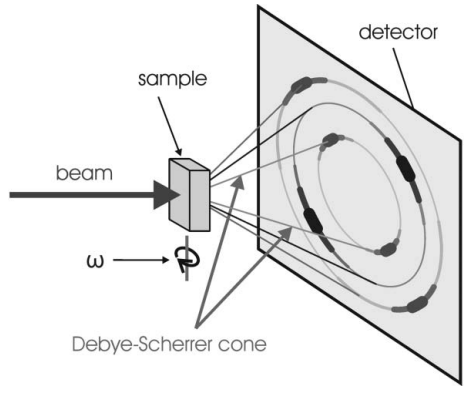

Figure 3
Schematic representation of the conventional texture step-scan technique. The sample is rotated in discrete steps around the orientation angle ω. At each position of the angle ω a diffraction image is taken.

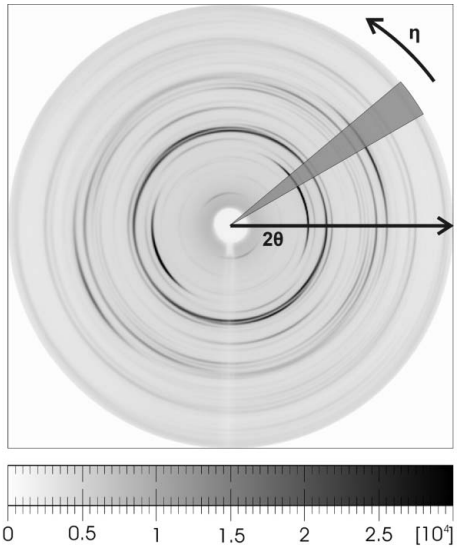

Figure 4
Diffraction diagram at $\omega = 0^\circ$ of human dental enamel. The diffraction image shows Debye–Scherrer rings with distinct maxima, resulting from the preferred orientation. The shadowed triangle marks an integration zone which is used for data evaluation.

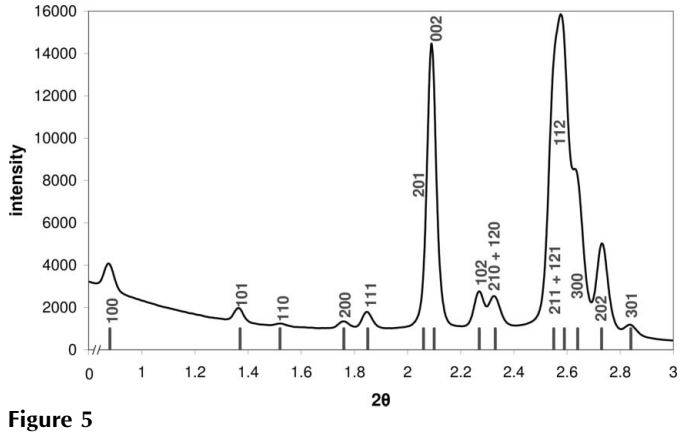

Figure 5
One-dimensional diffraction diagram calculated from the two-dimensional diffraction image shown in Fig. 4. The scan shows many overlapped peaks. The corresponding peak positions are marked and indexed for hydroxylapatite.

0.5 mm and the sample–detector distance was chosen as 1440 mm.

The texture measurements were carried out using the conventional step technique (Heidelbach *et al.*, 1999; Wcislak *et al.*, 2001, 2002; Lonardelli *et al.*, 2005; Klein, 2009). Diffraction images were taken at the orientation angle ω in the range $-80^\circ \leq \omega \leq +80^\circ$ in equiangular steps of $\Delta\omega = 5^\circ$; the exposure time was 20 s per image. Because of the sample geometry the full range of the orientation angle ω ($-90^\circ \leq \omega \leq +90^\circ$) is not accessible; complete pole figures were therefore calculated by means of mathematical texture analysis. Fig. 3 shows schematically this texture measurement technique with an area detector. A diffraction image for $\omega = 0^\circ$ (primary beam perpendicular to the sample surface) is shown in Fig. 4. Overlapping Debye rings can be seen with high maxima on the rings, resulting from the preferred orientation of the crystallites. The Bragg angle 2θ and the orientation angle η are marked. A typical integration zone used for data evaluation, triangle-like, is shadowed.

In Fig. 5 a one-dimensional diffraction diagram of the enamel is shown, calculated from the two-dimensional diffraction image in Fig. 4. It shows clearly the overlapping of diffraction peaks.

A set of data necessary to calculate the orientation distribution of one local measurement point consists of 33 two-dimensional diffraction images, at a step width in ω of 5°. There are 27 local grid points, so 891 diffraction images have been analysed in this study.

3.1. Mathematical texture analysis

The calculation of the quantitative texture analysis becomes more difficult if we deal with totally or partly overlapping reflection peaks. Fig. 5 shows a typical diffraction diagram of hydroxylapatite; it can be seen that a number of peaks overlap even though the material consists of only one phase. This is the reason for using a combined Rietveld texture analysis. We applied the program *MAUD* (Lutterotti *et al.*, 1997). *MAUD* is very much suitable for dealing with overlapping diffraction peaks even from different phases. In *MAUD* the orientation distribution function is calculated using the E-WIMV method [see Lutterotti *et al.* (2004), especially equation (2), and Lutterotti & Bortolotti (2005)], which is a modification of the numerical WIMV algorithm (Matthies & Vinel, 1982; Matthies & Wenk, 1985; Matthies *et al.*, 1997) which provides an automatic conditional ghost correction (Matthies, 1979).

A set of 33 two-dimensional diffraction images serves as input. Each image is divided in segments of, for example, 5° in η; these segments are integrated over the orientation angle η along the diffraction angle 2θ (Fig. 4). In this manner a set of 72 one-dimensional diffraction diagrams per diffraction image is constructed, which is used for the Rietveld analysis.

Each diffraction diagram contains, besides the intensities, specific information about the diffraction angle 2θ and the orientation angles ω and η. After the classical Rietveld refinement, differences between measured and calculated intensities occur if a texture is present. A texture-weight factor is then calculated using a Le Bail algorithm. These texture-weight factors together with the information of the angles ω, η and θ are the basis for the calculation of the orientation distribution function using the E-WIMV method, improving the Rietveld refinement fit. After this optimization process the final results are provided, such as experimental pole figures of considered reflections *hkl* and complete recalculated pole figures of measured and not measured *hkl*, inverse pole figures and the whole texture information given by the orientation distribution function as well as crystallographic parameters. The obtained fit can be compared with the actual data (Figs. 6 and 7) and the recalculated pole figures can be compared with the experimental ones (Fig. 8).

The Rietveld-texture analysis program *MAUD* is a powerful tool for analysing textures of biomaterials and engineering materials, dealing especially with low crystal symmetries, overlapping diffraction peaks and different

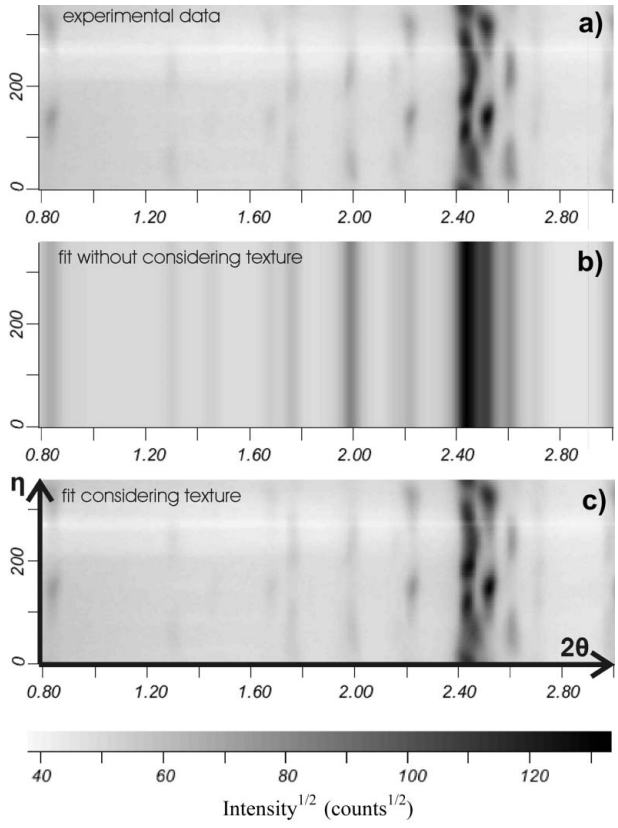

Figure 6
Result of a Rietveld-texture refinement for a diffraction image at $\omega = 0°$. The presentation of the two-dimensional data is made in orthogonal coordinates. (*a*) Experimental data; diffraction lines show minima and maxima. (*b*) Rietveld fit without consideration of the texture; diffraction lines have constant intensities. (*c*) Rietveld-texture refinement with consideration of the texture; diffraction lines show minima and maxima.

phases. Exemplarily, the results of a Rietveld analysis of a two-dimensional diffraction image taken at $\omega = 0°$ are shown in Fig. 6. A Rietveld-texture refinement of a single integrated one-dimensional segment of the same two-dimensional diffraction image is plotted in Fig. 7. The corresponding weighted *R*-value of this fit was 10.99%. The refined lattice parameters for HAP are a = 9.424 Å and c = 6.876 Å. The space group used was $P6_3/m$.

3.2. Calculation of anisotropic properties

The calculation of anisotropic properties from texture data was performed using the program package *Beartex* (Wenk *et al.*, 1998). Hereby one can directly use texture data received with *MAUD*. The *Beartex* routines 'tens' and 'velo' were used especially to calculate second- and fourth-rank tensor macroscopic properties such as thermal expansion and elastic modulus.

The macroscopic property $\overline{S}_{ijkl}$ of a polycrystalline aggregate is thereby given by the weighted average of the single-crystal coefficients S_{ijkl} (Bunge, 1993; Park *et al.*, 2001). The orientation distribution function $f(g)$ thus appears as the weight function of the average values of orientation-dependent physical properties,

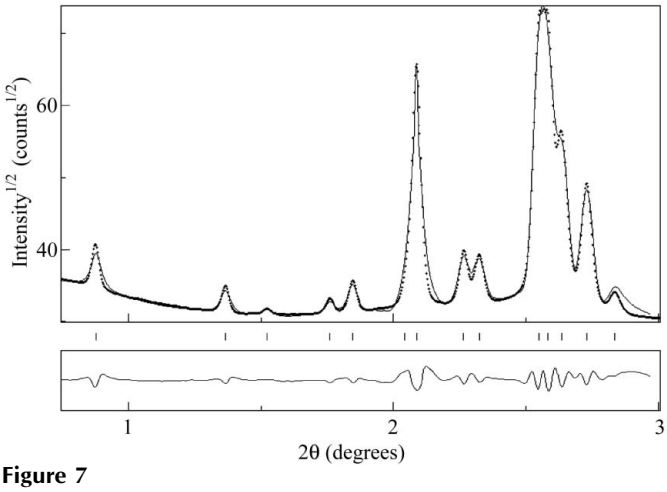

Figure 7
One-dimensional diffraction diagram of a single integrated segment (Fig. 4) after Rietveld-texture refinement. Crosses mark the measured data points; the continuous line represents the fitting. In the lower part the difference curve is shown.

$$\overline{S}_{ijkl} = \int S_{ijkl}(g) f(g)\ \mathrm{d}g. \tag{1}$$

This is a simple mean value neglecting the crystal interaction in the polycrystalline aggregate. The true mean value $\tilde{S}_{ijkl}$ depends on the orientation g of a considered crystal but also on the size, arrangement and orientation of its neighbouring crystals. To calculate the true mean value in the case of elastic properties several theories have been proposed. An approximation to the true average can be obtained for elastic properties using two formulations of Hooke's law,

$$\begin{aligned} \varepsilon_{ij} &= S_{ijkl}(g)\,\sigma_{kl}, \\ \sigma_{ij} &= C_{ijkl}(g)\,\varepsilon_{kl}, \end{aligned} \tag{2}$$

with $C_{ijkl} = (S_{ijkl})^{-1}$. This leads to the averages

$$\begin{aligned} \bar{S}^{R}_{ijkl} &= \int S_{ijkl}(g) f(g)\ \mathrm{d}g \quad \text{(Reuss)}, \\ \bar{C}^{V}_{ijkl} &= \int C_{ijkl}(g) f(g)\ \mathrm{d}g \quad \text{(Voigt)}. \end{aligned} \tag{3}$$

These two extreme cases of grain structure were formulated by Reuss (1929) and Voigt (1928). Normally, neither of these cases is realistic. Grains are quite often equiaxed. Then the averages of these two extreme values (Hill, 1952) can be used. The Hill averages are usually very close to the true polycrystal values and have therefore also been used for the calculations in this paper.

The single-crystal property is, in the case of thermal expansion (second-rank tensor), given by the coefficients of thermal expansion a_{ij}, and, in the case of the elastic modulus (fourth-rank tensor), by the elastic constants c_{ij}, each corresponding to the respectively measured material. Material constants like a_{ij} and c_{ij} can be found tabulated for various materials (Landolt Börnstein, 1992; *International Critical Tables of Numerical Data, Physics, Chemistry and Technology*, 1930).

The result of the first calculation step with 'tens' is a texture-weighted second- or fourth-rank tensor of the anisotropy for a given property. The program 'velo' uses the fourth-rank-

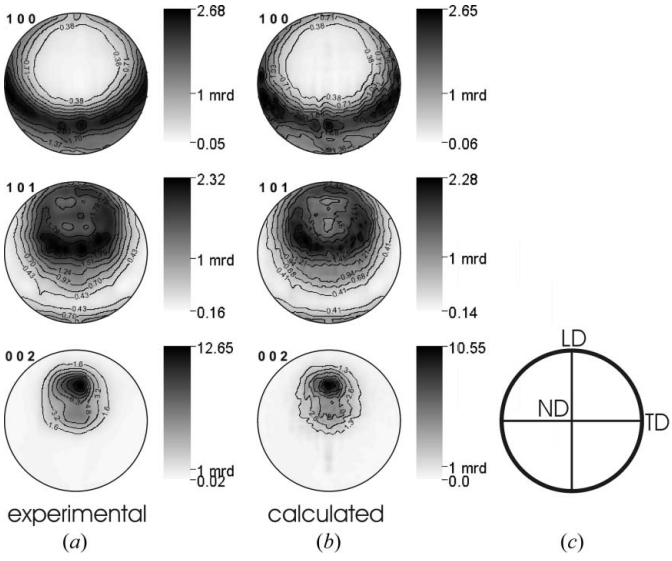

Figure 8
Experimental (*a*) and calculated (*b*) pole figures of the crystal planes (100), (101) and (001) for the marked measurement-grid point shown in Fig. 2. The sample coordinate system for the pole figures (ND: normal direction; LD: longitudinal direction; TD: transversal direction) is given in (*c*).

weighted tensor to calculate direction-dependent properties such as the elastic modulus. In the case of a texture-weighted second-rank property tensor received from 'tens', this tensor can be transformed into a direction-dependent property as shown in the following.

The resulting texture-weighted second-rank tensor aw_{ij} possesses information about the direction-dependent property $P_{(x,y,z)}$,

$$P_{(x,y,z)} = aw_{11}\cdot x\cdot x + aw_{22}\cdot y\cdot y + aw_{33}\cdot z\cdot z + 2aw_{12}\cdot x\cdot y + 2aw_{13}\cdot x\cdot z + 2aw_{23}\cdot y\cdot z. \quad (4)$$

The optional conversion of the Cartesian coordinates x,y,z into polar coordinates α,β for a stereographic projection is given by

$$\begin{aligned} x &= \sin\alpha\cdot\cos\beta,\\ y &= \sin\alpha\cdot\sin\beta,\\ z &= \cos\alpha. \end{aligned} \quad (5)$$

4. Results

4.1. Calculation of the texture

As described above, the Rietveld-texture analysis using the program *MAUD* was used to calculate pole figures from the two-dimensional diffraction data. Experimental and recalculated pole figures of the marked measurement-grid point (Fig. 2) are shown in Fig. 8. A comparison of both pole figures sets shows that the quality and the reliability of the Rietveld-texture refinement are very good. Former investigations of human dental enamel pointed out that an interpretation of a (001) pole figure is sufficient to describe changes in texture (Raue & Klein, 2010), because the orientation of the crystallites can be explained by a rotational symmetric fibre texture; the fibre axis itself is hereby parallel to the *c*-axis of the crystallites (Raue, 2008; Raue & Klein, 2010).

The sample coordinate system in the stereographic projection is given in Fig. 8(*c*). In order to correlate the directional results to the sample, the sample normal (ND) in Fig. 2 is perpendicular to the image plane and the longitudinal direction (LD) lies parallel to the image plane pointing upwards.

The local variation of the orientation of the HAP crystallites within the sample is illustrated in Fig. 9. The upper row (*a*) shows the orientation change of the (001) poles in the horizontal direction, the lower one (*b*) in the vertical direction. It can be clearly seen that the local orientation in the horizontal sample direction changes almost symmetrically and continuously from the left side of the sample to the right side. In the vertical sample direction a local change from the normal to the longitudinal direction can be seen. Even the orientation densities change locally, as shown in Fig. 10(*a*) for the horizontal path and in Fig. 10(*b*) for the vertical path.

These results imply that the dental enamel prisms, which are built up by stacking of (001) crystal planes along the long axis of the prisms with a free rotation of this plane around their normal, are tilted from the left to the right side in the incisor tooth (Raue, 2008; Raue & Klein, 2010). In the vertical direction the prisms show a tilting from the normal to the longitudinal direction.

4.2. Calculation of the anisotropic elastic modulus and thermal expansion

The result of texture analysis, *i.e.* the orientation distribution function, is the basis for any property calculation. Hence,

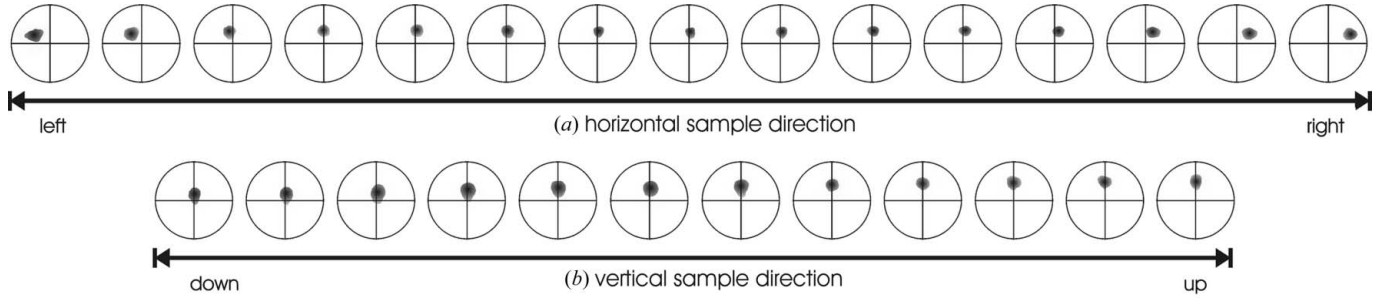

Figure 9
Local change of the orientation of the (001) poles of HAP in a human incisor tooth; (*a*) horizontal, (*b*) vertical sample direction (*cf.* Fig. 2).

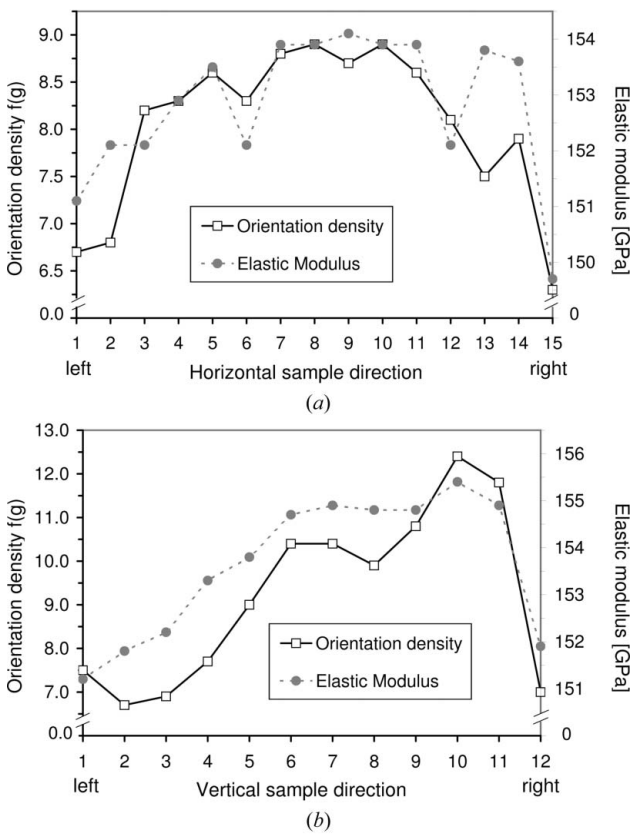

Figure 10
Local change of the orientation densities and the maximum values of the anisotropic elastic modulus (dotted lines) in the horizontal (*a*) and vertical (*b*) sample directions. The orientations of these maxima are directly comparable with those of the (001) poles (Fig. 9).

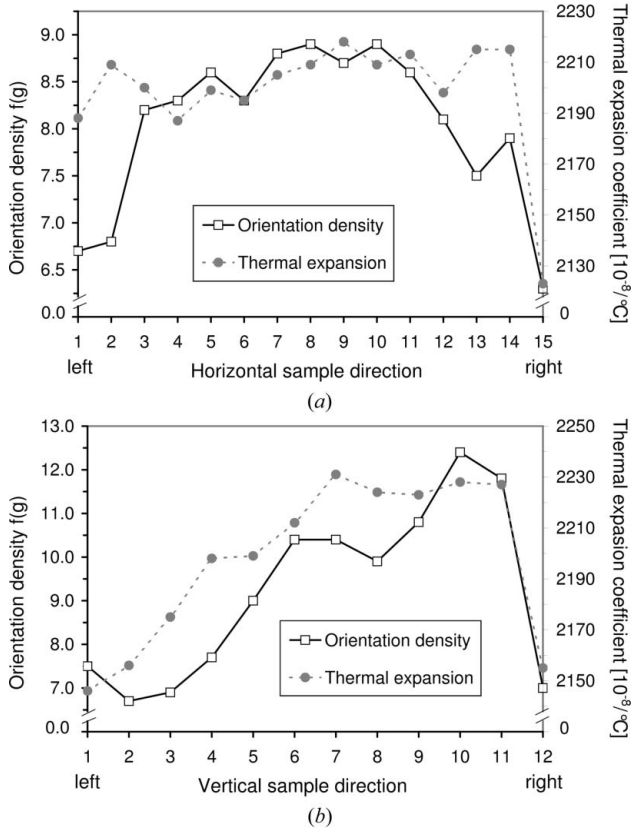

Figure 11
Texture-calculated maximum values of the thermal expansion in the horizontal (*a*) and vertical (*b*) sample direction (dotted lines). Additionally the orientation densities are given.

there is a general correlation of preferred orientations with anisotropic properties (Bunge, 1993; Park *et al.*, 2001). It is not astonishing that the directional maxima of elastic modulus show the same behaviour as the orientation of the corresponding (001) poles (again representing the texture). The local values in the horizontal sample direction of the elastic modulus are represented in Fig. 10(*a*); those of the vertical sample direction are shown in Fig. 10(*b*).

As well as the anisotropic behaviour of the elastic modulus, the thermal expansion originates from texture. Likewise the maxima of thermal expansion are similarly oriented (*cf.* pole figures in Fig. 9).

The resulting local maximum values are shown in Fig. 11(*a*) for the horizontal and in Fig. 11(*b*) for the vertical sample directions.

5. Conclusion

The physical properties of human dental enamel are of prime importance for therapies, inlays and dentures. Only a few investigations have been performed and the crystallographic texture has been described as 'highly complex' (Al-Jawad *et al.*, 2007; Dorozhkin, 2007; LeGeros, 1991). The whole three-dimensional direction dependence of physical properties such as the elastic modulus has mostly been reduced to one or two specific directions [*e.g.* the elastic modulus from indentation measurements such as by Xie *et al.* (2009), Cuy *et al.* (2002) or Braly *et al.* (2007), to mention only some].

Applying diffraction and calculation methods used in materials science for polycrystalline materials in order to determine real three-dimensional anisotropic properties are steps towards the goal of determining the anisotropic properties for any location in teeth. Here we have presented methods to obtain detailed local information about the crystalline structure, the orientation and anisotropic properties of dental enamel. Dental enamel is made of crystalline hydroxylapatite and, owing to its crystal structure, its diffraction diagram shows multiple overlapping peaks. This makes a texture and structure analysis difficult, but this problem can be easily overcome by modern Rietveld-texture refinements.

Because of its high angular and local resolving power and brilliance, high-energy synchrotron radiation in combination with an area detector was used. The methods to measure and to analyse textures quantitatively were directly adopted from those used in materials science (Bunge, 1993; Wenk *et al.*, 1998; Lutterotti *et al.*, 1997; Wcislak *et al.*, 2001; Bunge *et al.*, 2003; Klein, 2009). The results show that human dental enamel is strongly textured, more than 12 times random, and beyond that a strong local change of the orientation in a tooth exists. The texture as well as physical properties (elastic modulus and thermal expansion) are directly connected to the application

profile of a tooth (maximum load during chewing from the direction of the opposite tooth). From local measurement results it arises that dental enamel prisms are approximately perpendicularly oriented to the tooth surface with an inclining tilt towards the top of the tooth.

The anisotropy of these properties can thus be compared and evaluated in contrast to the properties of materials used to fill cavities. All these results give a lot of new information about dental enamel and the properties new filling materials should possess. The focus of this article lies in the procedures for obtaining orientation-dependent information from dental enamel, such as the anisotropic elastic modulus and anisotropic thermal expansion. A detailed presentation of results of similar measurements and calculations on common dental filling materials as well as on dental enamel, together with a literature review and our own indentation measurements (obtaining the elastic modulus by a different method), will be given in another paper.

The authors acknowledge financial support for this project from the Deutsche Forschungsgemeinschaft (DFG) and HASYLAB/DESY for beam time. The help of Dr H. Sowa, Ms I. Janßen and Dipl.-Geow. C. Hartmann (all GZG, University of Göttingen) is also acknowledged. The authors are also grateful to Dr N. Gersdorff and Dr M. Rödiger (University Clinical Center Göttingen, ZMK) for help, discussion and providing sample material, and to Dr K. Ullemeyer (IFM-GEOMAR, University of Kiel, Germany) for discussions.

References

Al-Jawad, M., Steuwer, A., Kilcoyne, S. H., Shore, R. C., Cywinski, R. & Wood, D. J. (2007). *Biomaterials*, **28**, 2908–2914.

Braly, A., Darnell, L. A., Mann, A. B., Teaford, M. F. & Weihs, T. P. (2007). *Arch. Oral Biol.* **52**, 856–860.

Bunge, H.-J. (1993). *Texture Analysis in Materials Science*, 2nd ed. Göttingen: Cuvillier Verlag.

Bunge, H. J., Wcislak, L., Klein, H., Garbe, U. & Schneider, J. R. (2003). *J. Appl. Cryst.* **36**, 1240–1255.

Chudoba, T., Heuer, D., Schwarzer, N. & Zubko, P. (2005). *Qualitätsbewertung einiger kommerzieller Komposit-Zahnfüllmaterialien*, http://www.esae.de/zahn.html.

Cuy, J. L., Mann, A. B., Livi, K. J., Teaford, M. F. & Weihs, T. P. (2002). *Archs. Oral Biol.* **47**, 281–291.

Dorozhkin, S. V. (2007). *J. Mater. Sci.* **42**, 1061–1095.

Heidelbach, F., Riekel, C. & Wenk, H.-R. (1999). *J. Appl. Cryst.* **32**, 841–849.

Hill, R. (1952). *Proc. Phys. Soc. A*, **65**, 349–354.

International Critical Tables of Numerical Data, Physics, Chemistry and Technology (1930). Vol. III. New York: McGraw-Hill.

Klein, H. (2009). *Adv. Eng. Mater.* **11**, 452–458.

Landolt-Börnstein (1992). *Numerical Data and Functional Relationships in Science and Technology, New Series*, Vol. III/29a. Berlin: Springer.

LeGeros, R. Z. (1991). *Calcium Phosphates in Oral Biology and Medicine.* Basel: Karger.

Lonardelli, I., Wenk, H.-R., Lutterotti, L. & Goodwin, M. (2005). *J. Synchrotron Rad.* **12**, 354–360.

Lutterotti, L. & Bortolotti, M. (2005). *Acta Cryst.* A**61**, C158–C159.

Lutterotti, L., Chateigner, D., Ferrari, S. & Ricote, J. (2004). *Thin Solid Films*, **450**, 34–41.

Lutterotti, L., Matthies, S., Wenk, H.-R., Schultz, A. J., Richardson, J. (1997). *J. Appl. Phys.* **81**, 594–600.

Matthies, S. (1979). *Phys. Status Solidi B*, **92**, K135–K138.

Matthies, S., Lutteroti, L. & Wenk, H. R. (1997). *J. Appl. Cryst.* **30**, 31–42.

Matthies, S. & Vinel, G. W. (1982). *Phys. Status Solidi B*, **112**, K111–K114.

Matthies, S. & Wenk, H.-R. (1985). *An Introduction to Modern Texture Analysis*, edited by H.-R. Wenk, ch. 7, pp. 139–147. Orlando: Academic Press.

Nye, J. F. (1985). *Physical Properties of Crystals.* Oxford University Press.

Park, N. J., Klein, H. & Dahlem-Klein, E. (2001). *Program System: Physical Properties of Textured Materials*, 2nd ed., edited by H. J. Bunge. Göttingen: Cuvillier Verlag.

Raue, L. (2008). Doctoral thesis, RWTH Aachen, Germany.

Raue, L. & Klein, H. (2010). *Solid State Phenom.* **160**, 281–286.

Reuss, A. (1929). *Z. Angew. Math. Mech.* **9**, 49–58.

Voigt, W. (1928). *Lehrbuch der Kristallphysik.* Leipzig: Teubner.

Wcislak, L., Klein, H., Bunge, H. J., Garbe, U., Tschentscher, T. & Schneider, J. R. (2002). *J. Appl. Cryst.* **35**, 82–95.

Wcislak, L., Schneider, J. R., Tschentscher, T., Klein, H. & Bunge, H. J. (2001). *Nucl. Instrum. Methods Phys. Res. A*, **476–478**, 1257–1260.

Wenk, H.-R., Matthies, S., Donovan, J. & Chateigner, D. (1998). *J. Appl. Cryst.* **31**, 262–269.

Xie, Z.-H., Swain, M. V., Swadener, G., Munroe, P. & Hoffman, M. (2009). *J. Biomech.* **42**, 1075–1080.